The FreeEOS Code for Calculating the Equation of State for Stellar Interiors I: An Improved EFF-Style Approximation for the Fermi-Dirac Integrals

Alan W. Irwin

Department of Physics and Astronomy, University of Victoria,
P.O. Box 3055, Victoria, British Columbia, Canada, V8W 3P6
Electronic mail: irwin@beluga.phys.uvic.ca

ABSTRACT

I present a modified form of the Eggleton, Faulkner, and Flannery approximation to Fermi-Dirac integrals that substantially reduces the non-relativistic fitting errors. This new approximation has been incorporated into FreeEOS (http://freeeos.sourceforge.net/), a software package for calculating the equation of state using an efficient free-energy minimization technique that is suitable for physical conditions in stellar interiors.

Subject headings: equation of state — stellar interiors — stellar evolution

1. Introduction

FreeEOS is a software package for calculating the equation of state (hereafter, EOS) using an efficient free-energy minimization technique that is suitable for physical conditions in stellar interiors. This paper is the first in a series detailing various aspects of the FreeEOS implementation. Here, the approximations for the Fermi-Dirac integrals are presented.

Eggleton, Faulkner, and Flannery (1973, hereafter EFF) published an important paper on the EOS for stellar material that included an approximation for Fermi-Dirac integrals for all degeneracies and temperatures. This approximation, which has seen wide-spread use in stellar-interior calculations, has been slightly modified by Pols et al., 1995 (hereafter PTEH) to avoid some significance loss in the entropy approximation, and we refer to this collected work as the EFF approximation. The chief advantages of this approximation are the following: it is mathematically continuous; it can be rapidly evaluated with reasonable precision; and it gives thermodynamically consistent results for all degeneracies and temperatures.

I present in this paper an improvement to the EFF approximation that preserves these advantages while giving substantially improved accuracy for the important non-relativistic case as illustrated by a number of different FreeEOS calculations.

2. Approximation to P_e

I derive in this section an approximation form for P_e, the pressure associated with an ideal gas of free electrons. We focus on P_e here because other thermodynamic functions for ideal free electrons can be derived from P_e by well-known thermodynamic relationships (see Sect. 4). Except for the new non-relativistic result at the end of this section, the material presented here has also been covered by EFF.

From equation (24.99) of Cox and Giuli (1968, hereafter CG) and equation (21) of EFF, we have the following result:

$$\frac{\lambda_c^3}{8\pi m_e c^2} P_e \equiv P_\star(\eta,\beta) = \frac{2\sqrt{2}}{3}\beta^{5/2}[F_{3/2}(\eta,\beta) + (1/2)\beta F_{5/2}(\eta,\beta)], \tag{1}$$

where the Compton wavelength is defined by $\lambda_c \equiv h/(m_e c)$, η is a degeneracy parameter, $\beta \equiv kT/(m_e c^2)$, and $F_k(\eta,\beta)$ are Fermi-Dirac integrals defined by

$$F_k(\eta,\beta) \equiv \int_0^\infty \frac{x^k[1+(1/2)\beta x]^{1/2}\mathrm{d}x}{\exp(x-\eta)+1} \tag{2}$$

(see eq. (24.97) of CG).

From equations (24.257), (24.271), and (24.207) of CG, we find the following general form of expansions for $P_\star$:

$$P_\star \simeq \beta^{5/2}\exp(\eta)\sum_{m,n=0} d^{(1)}_{m,n}\exp(m\eta)\beta^n \quad (\eta \ll -1, \beta \ll 1), \tag{3}$$

$$P_\star \simeq \beta^{4}\exp(\eta)\sum_{m,n=0} d^{(2)}_{m,n}\exp(m\eta)\beta^{-n} \quad (\eta \ll -1, \beta \gg 1), \tag{4}$$

$$P_\star \simeq (\eta\beta)^{5/2}\sum_{m,n=0} d^{(3)}_{m,n}\eta^{-2m}(\eta\beta)^n \quad (\eta \gg 1, \eta\beta \ll 1), \tag{5}$$

and

$$P_\star \simeq (\eta\beta)^{4}\sum_{m,n=0} d^{(4)}_{m,n}\eta^{-2m}(\eta\beta)^{-n} \quad (\eta \gg 1, \eta\beta \gg 1), \tag{6}$$

where $d^{(k)}_{m,n}$ are well-known numerical coefficients. Following EFF, high-order terms in $\ln(\beta)$ for equation (4) and in $\ln(\eta\beta)$ for equation (6) have been ignored. Furthermore, if we define the fitting variables f and g by

$$\eta \equiv 2\sqrt{1+f} + \ln\frac{\sqrt{1+f}-1}{\sqrt{1+f}+1} \tag{7}$$

and

$$g \equiv \beta\sqrt{1+f}, \tag{8}$$

then the approximation form,

$$P_\star \simeq \frac{f}{1+f} g^{5/2}(1+g)^{3/2}\frac{\sum_{m=0}^{M-1}\sum_{n=0}^{N-1}\widehat{P}_{m,n} f^m g^n}{(1+f)^{M-1}(1+g)^{N-1}}, \tag{9}$$

reduces to the form of the limiting approximations given by equations (3) through (6) for the four limits ($f \ll 1, g \ll 1$); ($f \ll 1, g \gg 1$); ($f \gg 1, g \ll 1$); and ($f \gg 1, g \gg 1$).

EFF determined the coefficients $\widehat{P}_{m,n}$ of equation (9) (see their eq. [22]) through the method of least squares. The resulting fits are useful for all values of f and g, but of course there are fitting errors even at the limits, and in particular the non-relativistic limit. To improve the accuracy of the fit close to this limit, I have used (with $k_{\rm NR} = 1$) the following generalized approximation form:

$$P_\star \simeq k_{\rm NR} P_\star^{\rm NR} + \frac{f}{1+f} g^{5/2} (1+g)^{3/2} \frac{\sum_{m=0}^{M-1} \sum_{n=k_{\rm NR}}^{N-1} \widehat{P}_{m,n} f^m g^n}{(1+f)^{M-1}(1+g)^{N-1}}, \tag{10}$$

where the non-relativistic limit of $P_\star$ is defined by

$$P_\star^{\rm NR} \equiv \frac{2\sqrt{2}}{3} \frac{(1+g)^{3/2}}{(1+g)^{N-1}} \beta^{5/2} F_{3/2}(\eta), \tag{11}$$

and $F_{3/2}(\eta) \equiv F_{3/2}(\eta, 0)$. $k_{\rm NR}$ is a control variable that is either set to 0 or 1. $k_{\rm NR} = 0$ (where, for example, eq. [10] reduces to eq. [9]) corresponds to the case where the non-relativistic component has not been separated, and $k_{\rm NR} = 1$ corresponds to the case when the non-relativistic component of the approximation has been separated.

The form of $P_\star^{\rm NR}$ has been carefully chosen to mimic the g-dependence of the $n = 0$ terms of equation (9). This means for $k_{\rm NR} = 1$ the sum over n in equation (10) can start at $n = 1$, and for $n \geq 1$ the $\widehat{P}_{m,n}$ coefficients determined by the method of least squares using either $k_{\rm NR} = 0$ or 1 are numerically quite similar to each other. In practice, $P_\star^{\rm NR}$ is approximated using the Cody-Thacher (1967) approximation for $F_{3/2}(\eta)$. For $k_{\rm NR} = 1$ and $g \ll 1$, the second term of equation (10) becomes negligible relative to the first so the fitting errors close to this limit (and also for solar conditions) approach the errors of the Cody-Thacher approximation which are smaller than 1 part in 10^8 (see Fig. 1 where I have compared results from the Cody-Thacher approximation and precise numerical integration).

3. Other Fermi-Dirac Integrals

A complete EOS requires calculation of n_e, s_e, and u_e, the number, entropy, and internal energy per unit volume of ideal free electrons. From equation (24.98) of CG and equation (1) of EFF we have the following result:

$$\frac{\lambda_c^3}{8\pi} n_e \equiv \varrho_\star(\eta, \beta) = \sqrt{2}\, \beta^{3/2} [F_{1/2}(\eta, \beta) + \beta F_{3/2}(\eta, \beta)]. \tag{12}$$

Furthermore, to reduce numerical significance loss when calculating s_e at high degeneracy (see also Appendix A in PTEH), we calculate the auxiliary thermodynamic quantity $Q_\star$ defined by

$$Q_\star \equiv \beta \frac{\partial P_\star(\eta, \beta)}{\partial \beta} - 2\sqrt{1+f}\, \frac{\partial P_\star(\eta, \beta)}{\partial \eta}. \tag{13}$$

The entropy and internal energy of the free electrons may be calculated from $\varrho_\star$ and $Q_\star$ using

$$\frac{s_e}{n_e k} \equiv s_\star(\eta,\beta) = \frac{Q_\star}{\beta\varrho_\star} + 2\sqrt{1+f} - \eta = \frac{Q_\star}{\beta\varrho_\star} + \ln\left[\frac{(1+\sqrt{1+f}\,)^2}{f}\right] \tag{14}$$

and

$$\frac{\lambda_c^3}{8\pi m_e c^2} u_e \equiv u_\star(\eta,\beta) = Q_\star + 2g\varrho_\star - P_\star. \tag{15}$$

(See eqs. [A4] and [A5] of PTEH with T in those equations replaced by $\beta \equiv kT/(m_e c^2)$ to be consistent with the notation of the rest of the PTEH paper.)

4. Thermodynamically Consistent Approximations

Our adopted approximation forms for $\varrho_\star$ and $Q_\star$ are

$$\varrho_\star \simeq k_{\rm NR}\varrho_\star^{\rm NR} + \frac{f}{1+f} g^{3/2}(1+g)^{3/2} \frac{\sum_{m=0}^{M}\sum_{n=k_{\rm NR}}^{N} \widehat{\varrho}_{m,n} f^m g^n}{(1+f)^M (1+g)^N} \tag{16}$$

and

$$Q_\star \simeq k_{\rm NR} Q_\star^{\rm NR} + \frac{f}{(1+f)^2} g^{5/2}(1+g)^{3/2} \frac{\sum_{m=0}^{M}\sum_{n=k_{\rm NR}}^{N} \widehat{Q}_{m,n} f^m g^n}{(1+f)^M (1+g)^N}. \tag{17}$$

These approximation forms generalize equation (15) of EFF and equation (A3) of PTEH and allow us to separate out the non-relativistic component ($k_{\rm NR} = 1$) or not ($k_{\rm NR} = 0$). The index range for the sums in these approximations is determined by the index range for the sums in equation (10) and the relationships for $\widehat{\varrho}_{m,n}$ and $\widehat{Q}_{m,n}$ which we derive later (see eqs. [23] and [24]).

An alternative equation for $P_\star$ that is exactly equivalent to equation (10) is the following:

$$P_\star \simeq k_{\rm NR} P_\star^{\rm NR} + \frac{f}{1+f} g^{5/2}(1+g)^{3/2} \frac{\sum_{m=0}^{M}\sum_{n=k_{\rm NR}}^{N} \widehat{P'}_{m,n} f^m g^n}{(1+f)^M (1+g)^N}, \tag{18}$$

where $P_\star^{\rm NR}$ is given by equation (11), and

$$\widehat{P'}_{m,n} = \widehat{P}_{m,n} + \widehat{P}_{m-1,n} + \widehat{P}_{m,n-1} + \widehat{P}_{m-1,n-1}. \tag{19}$$

The $P_\star$ approximation form given by equation (18) is the same order as the approximations for $\varrho_\star$ and $Q_\star$ given by equations (16) and (17) so it is more convenient to use in an EOS calculation than equation (10) which is used for the fit.

To assure thermodynamic consistency with $P_\star$ we must have (see eq. [26] of EFF)

$$\varrho_\star \equiv \frac{1}{\beta}\frac{\partial P_\star(\eta,\beta)}{\partial \eta}. \tag{20}$$

When this equation and equation (13) are used in conjunction with equation (10) to specify the right-hand sides of equations (16) and (17) the following results are obtained:

$$\varrho_\star^{\rm NR} \equiv \frac{1}{\beta}\frac{\partial P_\star^{\rm NR}(\eta,\beta)}{\partial\eta} = \frac{P_\star^{\rm NR}}{\beta}\left[\frac{F'_{3/2}(\eta)}{F_{3/2}(\eta)} + \frac{5/2-N}{2}\frac{g}{1+g}\frac{f}{(1+f)^{3/2}}\right], \tag{21}$$

$$\begin{aligned} Q_\star^{\rm NR} &\equiv \beta\frac{\partial P_\star^{\rm NR}(\eta,\beta)}{\partial\beta} - 2\sqrt{1+f}\,\frac{\partial P_\star^{\rm NR}(\eta,\beta)}{\partial\eta} \\ &= P_\star^{\rm NR}\left[5/2 - \frac{2\sqrt{1+f}\,F'_{3/2}(\eta)}{F_{3/2}(\eta)} + \frac{5/2-N}{1+f}\frac{g}{1+g}\right], \end{aligned} \tag{22}$$

$$\begin{aligned} \widehat{\varrho}_{m,n} &= (m+1)\widehat{P}_{m,n} + [5/4 + n/2 + (m-M)]\widehat{P}_{m-1,n} \\ &\quad + (m+1)\widehat{P}_{m,n-1} + [2 + (n-N)/2 + (m-M)]\widehat{P}_{m-1,n-1}, \end{aligned} \tag{23}$$

and

$$\begin{aligned} \widehat{Q}_{m,n} &= (1/2 - 2m + n)\widehat{P}_{m,n} + [5/2 - 2(2m-M) + n]\widehat{P}_{m-1,n} \\ &\quad + [2 - 2m + (n-N)]\widehat{P}_{m,n-1} + [4 - 2(2m-M) + (n-N)]\widehat{P}_{m-1,n-1} \\ &\quad - 2(m-M-1)\widehat{P}_{m-2,n} - 2(m-M-1)\widehat{P}_{m-2,n-1}. \end{aligned} \tag{24}$$

Furthermore, it is straightforward to show these relationships and the preceding definitions satisfy the following well-known thermodynamic relationships:

$$n_e = \frac{1}{kT}\frac{\partial P_e(\eta,\beta)}{\partial\eta}, \tag{25}$$

$$\frac{s_e}{n_e k} \equiv \frac{u_e + P_e}{n_e kT} - \eta, \tag{26}$$

and

$$u_e = \frac{\beta\partial P_e(\eta,\beta)}{\partial\beta} - P_e. \tag{27}$$

In sum, the coefficients $\widehat{P}_{m,n}$ determined by the method of least squares (see below) and equations (1), (10), (12), (14) – (19), and (21) – (24) yield a thermodynamically consistent set of approximations for P_e, n_e, s_e, and u_e.

5. Least-Squares Fitting Procedure

I determined the $\widehat{P}_{m,n}$ coefficients of the approximation form for $P_\star$ given in equation (10) using the method of least squares implemented with a singular-value decomposition technique based on the LAPACK *dgesvx* routine (see Anderson, et al. 1999). For the results reported here, it was

not necessary to edit out any of the singular values (i.e., this particular least-squares problem was well-conditioned, see discussion in Chapter 14.3 of Press et al, 1986).

I determined the values of $P_\star$ that were fitted using equations (1) and (2) and numerical integration of the appropriate Fermi-Dirac integrals. Those integrations were performed with a 4-point Gauss quadrature method that bisects the integration range a sufficient number of times to assure relative errors smaller than of 1 part in 10^9.

A number of different options were used for the least-squares fits reported in Section 7. I used two grids of f and g points for the fits; the original 8×7 grid given in section III of EFF for the ranges $-10.61 \leq \ln f \leq 7.82$ and $-7 \leq \ln g \leq 5$, and a much more extensive 61×61 equally spaced grid over the ranges $-15 \leq \ln f \leq 15$ and $-15 \leq \ln g \leq 15$. I used two weighting schemes for the least-squares fits. For the $k_{\rm NR} = 0$ case, I adopted the original EFF weighting scheme with a weight equal to $P_\star^{-2}$. These results should be largely equivalent to an unweighted non-linear least-squares fit of $\ln P_\star$. For the $k_{\rm NR} = 1$ case (with separated non-relativistic component), I adopted a weight equal to $\min(10^4 P_\star^{-2}, |P_\star - P_\star^{\rm NR}|^{-2})$. For large g, $P_\star^{\rm NR}$ is negligible relative to $P_\star$, and this weight approaches $P_\star^{-2}$. For small g, $|P_\star - P_\star^{\rm NR}|^{-2}$ becomes large (because the relative differences between the Cody-Thacher approximation used to calculate $P_\star^{\rm NR}$ and the precise numerical integration used to calculate $P_\star$ are less than 10^{-8}, see Fig. 1), and the weight reduces to the limiting $10^4 P_\star^{-2}$ value. The factor of 10^4 used in this limiting value is a good compromise that reduces the residuals in the important low-g region without substantially increasing the residuals in the high-g region.

6. The FreeEOS Equation of State

Some of the following results require EOS calculations which are supplied by the FreeEOS code which has been made publically available at http://freeeos.sourceforge.net/ under the GNU General Public License (GPL). A full description of the FreeEOS code is in preparation (Irwin et al. 2004) so we will only summarize its principal characteristics here.

The EOS is calculated using an equilibrium-constant approach to minimize the Helmholtz free-energy. For realistic abundance mixtures, this approach greatly reduces the number of linear equations that must be solved per iteration so that the solution can be rapidly obtained. This speed makes it practical to call the EOS directly from the stellar-interior code without introducing the errors associated with interpolating EOS tables (Cassisi & Irwin 2004, see also Dorman, Irwin, & Pedersen 1991).

The equilibrium-constant approach gives numerical solutions of high quality with thermodynamic consistency which is typically better than 12 decimal digits. Intercomparison of results on different floating-point platforms also confirms there are typically 12 decimal digits of numerical precision or better in the FreeEOS results.

The equilibrium-constant approach allows great flexibility in the choice of free-energy model.

The present calculations use the "EOS1" option suite of FreeEOS which includes the following components: arbitrarily relativistic and degenerate free electrons (using results from the present work); excited electronic states; a Planck-Larkin occupation probability (Rogers 1986); a complete complement of ro-vibrational energy levels for the ground electronic state of H_2 (Irwin, 1987) and H_2^+; a pressure-ionization occupation probability formulation similar to that of Mihalas, Däppen, & Hummer (1988); the exchange effect for arbitrarily relativistic and degenerate electrons (Kapusta, 1989 and Kovetz, Lamb, & Van Horn 1972); and the Coulomb effect. The Coulomb effect is treated with the Debye-Hückel approximation in the weak coupling limit and an approximation (PTEH) of the multicomponent combination of the one-component plasma result (DeWitt, Slattery, & Chabrier 1996) in the strong-coupling limit. A spline fit is used to interpolate between the weak and strong coupling limits. The limits of the intermediate coupling region and the size of the interaction radii that characterize the pressure-ionization occupation probability are adjusted to fit the OPAL EOS tables distributed at ftp://www-phys.llnl.gov/pub/opal/eos/.

7. Results and Discussion

Figure 2 shows representative stellar-interior model loci in f and g (the degeneracy and relativity parameters defined by eqs.[7] and [8]) in order to give the following results some context. The f,g loci were determined from a FreeEOS calculation based on the run of ρ, T, and abundance ($\vec{\epsilon}$) values taken directly from the models. The principal (well-known) results illustrated here are that relativistic corrections are beginning to be important for advanced stages of evolution, and degeneracy effects are strong for lower main sequence models and the cores of advanced-evolution models. Also, there is a substantial decrease of degeneracy and relativistic effects caused by the helium core flash that drives the rapid changes between the red-giant-tip model and the clump-giant model.

I determined a set of $\widehat{P}_{m,n}$ coefficients using a least-squares fit with the original 8×7 grid of EFF fitting points, $k_{\rm NR} = 0$ (unseparated non-relativistic component), and $M, N = 3$. The corresponding thermodynamically consistent $\widehat{P'}_{m,n}$, $\widehat{\rho}_{m,n}$, and $\widehat{Q}_{m,n}$ coefficients were determined using equations (19), (23), and (24). The rounded results were identical to the appropriate data taken from Table 2 and 5 in EFF and Table A1 in PTEH, thus simultaneously verifying the present and previous methods of determining the fitted coefficients and the corresponding set of thermodynamically consistent coefficients. In addition, we found for these low-order results, that the fitting residuals were changed very little by fitting on the 61×61 grid. However, that larger grid did prove essential for determining reliable high-order results.

Figure 3 illustrates fitting residuals for the original EFF $\widehat{P}_{m,n}$ coefficients and $\widehat{P}_{m,n}$ coefficients (see Tables 1, 2, and 3) determined with the present least-squares technique for the 61×61 grid using a separated non-relativistic component ($k_{\rm NR} = 1$) for $M, N = 3$, $M, N = 5$, and $M, N = 8$. Thanks to the high-precision of the Cody-Thacher approximation (see Figure 1) used to calculate $P_\star^{\rm NR}$, fitting with a separated non-relativistic component gives much better accuracy than the original

EFF results for low g values while the maximum fitting errors for intermediate and high g values remain essentially identical. Also, low-order results already have good accuracy, and convergence is reliable (although somewhat slow) as the order of the fit is increased.

Figure 4 illustrates FreeEOS results for the important solar case. The overall minimum of Γ_1 near the outer boundary corresponds to the combined hydrogen and first helium ionization zone, and the secondary minimum of Γ_1 slightly deeper in the model corresponds to the second helium ionization zone. EOS errors due to Fermi-Dirac integral approximations drop profoundly right near the outer boundary because very few free electrons exist in the outermost part to the model where hydrogen is not ionized. Throughout the model the EOS errors due to the original EFF approximation are already roughly an order of magnitude smaller than known errors in the inferred solar sound speed (see Figure 1 of Basu et al. 2003). However, the present $k_{\rm NR} = 1$ approximations of the same order do much better with errors typically reduced by 2 orders of magnitude or more compared to the original EFF results and 3 orders of magnitude or more compared to the observational errors. Thus, the present lowest-order fitting coefficients from Table 1 should serve even the most exacting solar pulsational frequency calculations.

Results (not illustrated) for other stellar models are similar to the solar case with the present $k_{\rm NR} = 1; M, N = 3$ approximation resulting in EOS errors that are typically improved over the original EFF approximation by at least two orders of magnitude for main-sequence models and one order of magnitude for advanced evolutionary models.

8. Conclusion

I have presented in this paper an improvement to the EFF approximation for Fermi-Dirac integrals that greatly increases the accuracy in the non-relativistic case. This approximation has been implemented as part of the FreeEOS code (distributed under the GPL at http://freeeos.sourceforge.net) for calculating the EOS for stellar-interior conditions. A comparison with precise numerical integration results for the solar case shows that the EOS errors due to the present lowest-order approximation (see fitting coefficients of Table 1) are roughly 2 orders of magnitude smaller than the EOS errors due to the original EFF approximation and 3 orders of magnitude smaller than typical observational errors associated with structure inversions of solar pulsational frequency data. Thus, the present lowest-order approximation should be suitable for all foreseeable stellar-interior and pulsational calculation needs, and higher-order approximations based on the coefficients given in Tables 2 and 3 should be reserved for future needs that are not currently anticipated.

I thank Don VandenBerg for providing some representative model calculations using a preliminary version of the FreeEOS code; Forrest Rogers for drawing my attention to a public-domain routine developed at Lawrence Livermore National Laboratory for precise numerical integration of Fermi-Dirac integrals; and Richard Stallman, Linus Torvalds, and many other programmers

for the Gnu/Linux computer operating system that made it practical to develop the FreeEOS code. The figures of this paper have been generated with the PLplot scientific plotting package (http://www.plplot.org).

REFERENCES

Anderson, E., Bai, Z., Bischof, C., Blackford, S., Demmel, J. and Dongarra, J., Du Croz, J., Greenbaum, A., Hammarling, S., McKenney, A., & Sorensen, D. 1999, LAPACK Users' Guide, 3rd Ed. (Philadelphia: Society for Industrial and Applied Mathematics)

Basu, S., Christensen-Dalsgaard, J., Howe, R., Schou, J., Thompson, M.J., Hill, F., and Komm, R. 2003, ApJ, 591, 432

Cassisi, S., & Irwin, A.W. 2004, in preparation

Cody, W. J., & Thacher, H. C. Jr. 1967, Math. Comp., 21, 30; erratum, 1967, Math. Comp., 21, 525

Cox, J. P., & Giuli, R. T. 1968, Principles of Stellar Structure (New York: Gordon and Breach) (CG)

DeWitt, H., Slattery, W., & Chabrier, G. 1996, Physica B228, 21

Dorman, B., Irwin, A.W., & Pedersen, B.B. 1991, ApJ, 381, 228

Eggleton, P. P., Faulkner, J., & Flannery B. P. 1973, A&A, 23, 325 (EFF)

Irwin, A. W. 1987, A&A, 182, 348 (I87)

Irwin, A.W., Swenson, F.J., VandenBerg, D.A., & Rogers, F.J. 2004, in preparation

Kapusta, J. W. 1989, Finite Temperature Field Theory (Cambridge: Cambridge University Press)

Kovetz, A., Lamb, D. Q., & Van Horn, H. M. 1972, ApJ, 174, 109

Mihalas, D., Däppen, W., & Hummer, W. G. 1988, ApJ, 331, 815

Pols, O. R., Tout, C. A., Eggleton, P. P., & Han, Z. 1995, MNRAS, 274, 964 (PTEH)

Press, W.H., Flannery, B.P., Teukolsky, S.A., & Vetterling, W. T. 1986, Numerical Recipes (Cambridge, Cambridge University Press)

Rogers, F. J. 1986, ApJ, 310, 723

Fig. 1.— A comparison of P_e results calculated with the Cody-Thacher approximation and the results of precise (see text) numerical integration in the non-relativistic limit. The degeneracy parameter f is defined by equation (7).

Fig. 2.— A comparison of the loci of model stellar interiors as a function of the degeneracy and relativity parameters f and g that are defined by equations (7) and (8). The models were calculated for solar metallicity using the University of Victoria stellar-interior code and a preliminary version of FreeEOS. The model loci corresponding to main sequence models of 0.1, 0.3, and 1.0 $M_\odot$ and models of 1.0 $M_\odot$ evolved to the tip of the red-giant branch and to the initial clump-giant phase (zero-age horizontal branch of solar metallicity) are respectively labelled "0.1", "0.3", "1.0", "RGT", and "CG" .

Fig. 3.— Fitting residuals in P_e as a function of the degeneracy and relativity parameters f and g that are defined by equations (7) and (8).

Fig. 4.— EOS results for a solar model specified as the (fixed) run of ρ, T, and abundance ($\vec{\epsilon}$) as a function of relative radius r/R within the model. The first adiabatic exponent is defined by $\Gamma_1 \equiv \partial \ln P(\rho, s, \vec{\epsilon})/\partial \ln \rho$ where s is the entropy per unit mass. $\Delta \ln P$ and $\Delta \ln v_s^2$ are the relative change in calculated total pressure and square of the adiabatic sound speed for various Fermi-Dirac integral calculations. For the second and third panels, the dotted line corresponds to the difference between the original EFF $k_{\rm NR} = 0; M, N = 3$ results and precise (see text) numerical integration results while the solid line corresponds to the difference between $k_{\rm NR} = 1; M, N = 3$ results of the present work and precise numerical integration results.

Table 1. $\widehat{P}_{m,n}$ for $k_{\rm NR} = 1$; $M, N = 3$

	m		
n	0	1	2
1	5.5051486	9.1814586	3.3509116
2	3.6945576	5.1656731	1.3336029

Table 2. $\widehat{P}_{m,n}$ for $k_{\rm NR} = 1$; $M, N = 5$

			m		
n	0	1	2	3	4
1	10.1292483	38.2616936	53.9322152	33.2523591	7.6188636
2	17.0862052	61.9601529	83.0404668	48.4264382	10.1598500
3	12.9298674	45.2012106	57.6788896	31.6885718	6.0008022
4	3.6944790	12.5145345	15.2593039	7.9029001	1.3333607

Table 3. $\widehat{P}_{m,n}$ for $k_{\rm NR} = 1$; $M, N = 8$

	m							
n	0	1	2	3	4	5	6	7
1	17.0746137	116.7565267	341.6206921	554.9387132	538.7259249	314.3185834	101.1346265	14.0190497
2	54.4249544	367.3451784	1059.8746088	1695.6501699	1619.0830291	926.9575547	292.1522041	39.4157661
3	96.8834221	645.6603616	1837.1092878	2893.7518429	2716.2321541	1523.9549922	469.6022201	61.4703123
4	103.8633443	683.8297286	1919.5366558	2977.3218243	2746.4224691	1508.7658062	453.7688812	57.4341957
5	66.9606940	435.9384048	1208.1733455	1846.0041046	1674.0076566	899.8017708	263.7720349	32.1654442
6	24.0145386	154.7433006	423.8018745	638.2945138	569.3319258	299.3392925	85.4389791	10.0000358
7	3.6945283	23.5876169	63.9072327	94.9578227	83.3911452	42.8892970	11.9134229	1.3333330

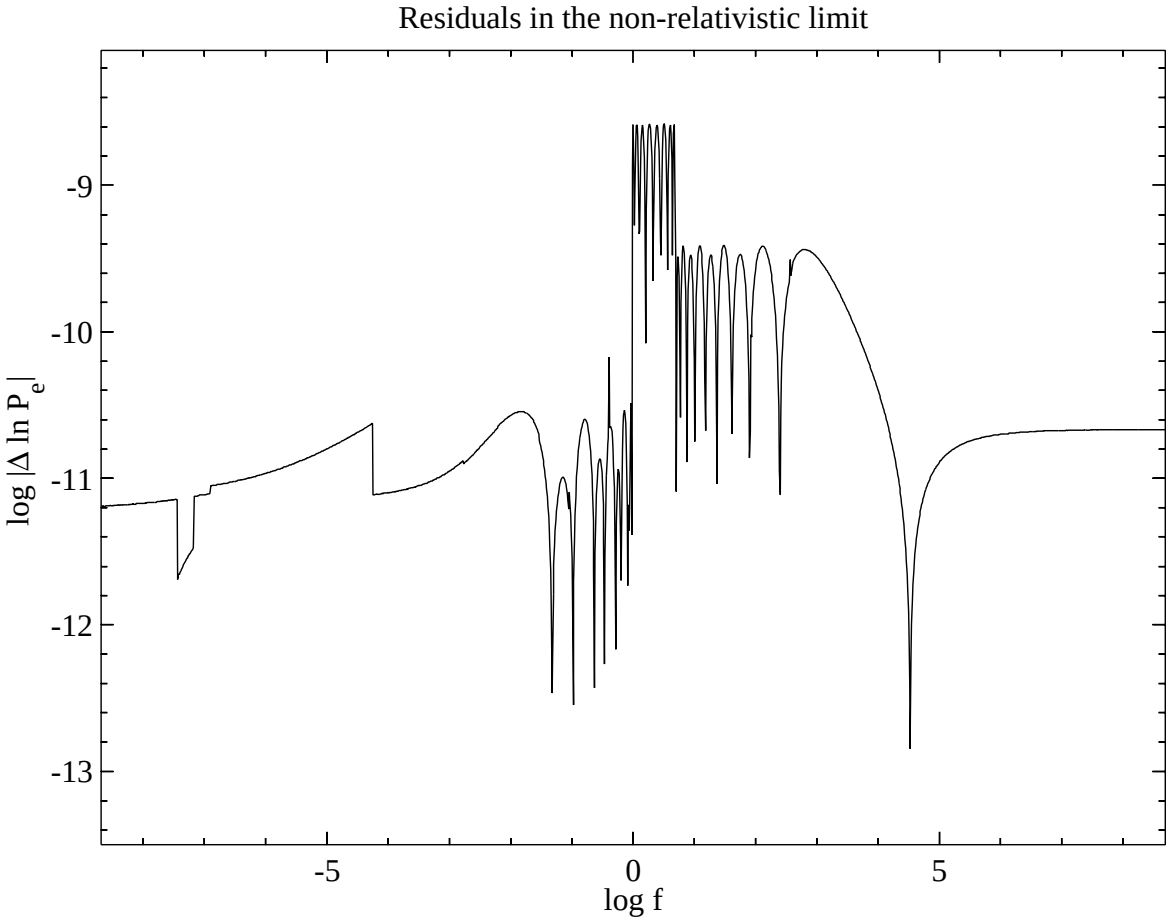
Residuals in the non-relativistic limit
log |Δ ln P_e|
-9
-10
-11
-12
-13
-5
0
5
log f

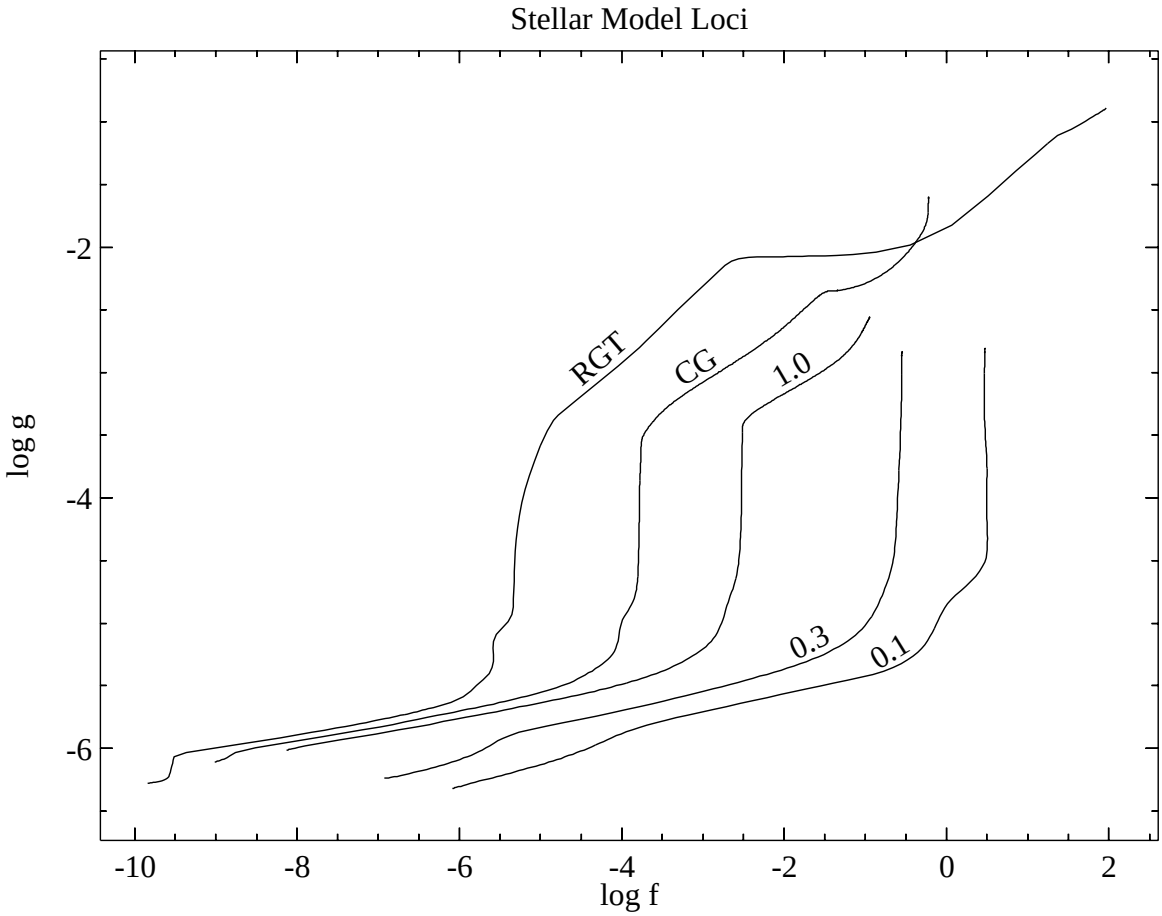
Stellar Model Loci
log g
log f
-2
-4
-6
-10
-8
-6
-4
-2
0
2
RGT
CG
1.0
0.3
0.1

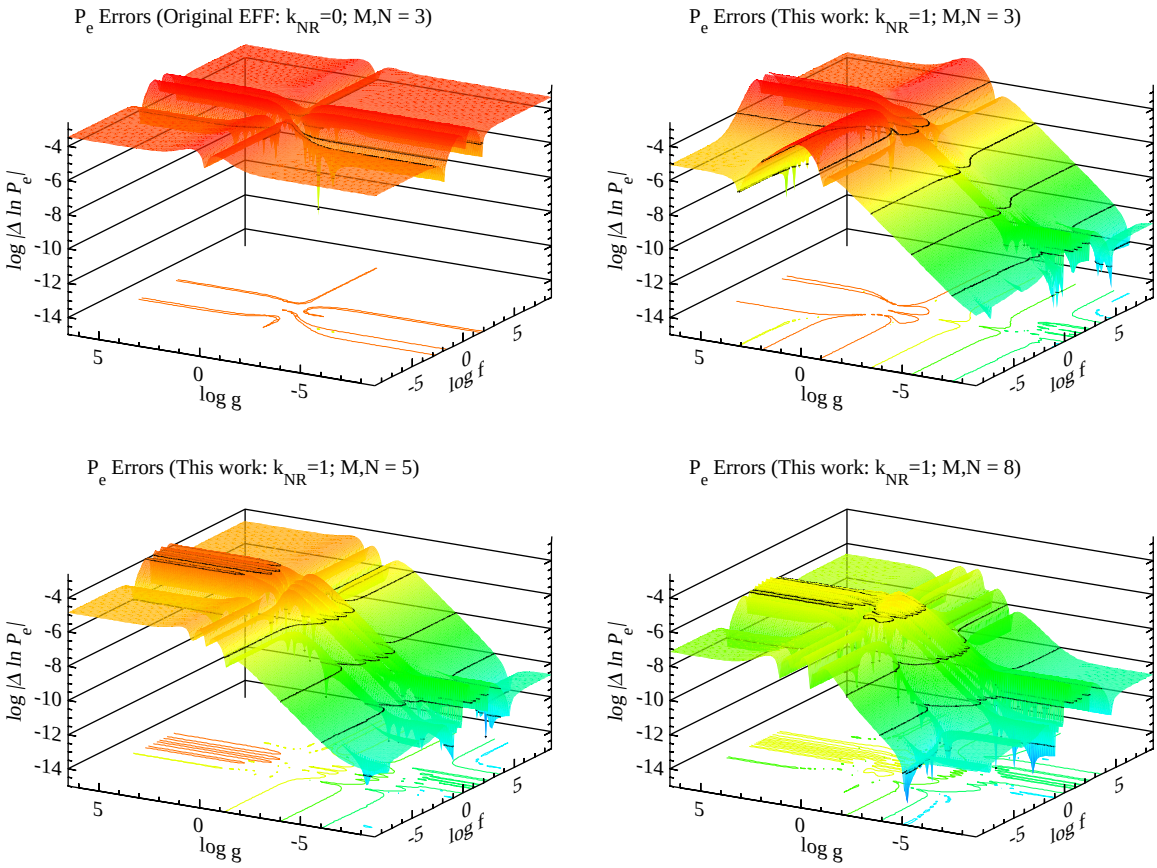
P_e Errors (Original EFF: k_NR=0; M,N = 3)
P_e Errors (This work: k_NR=1; M,N = 3)
P_e Errors (This work: k_NR=1; M,N = 5)
P_e Errors (This work: k_NR=1; M,N = 8)
log |Δ ln P_e|
-4
-6
-8
-10
-12
-14
5
0
-5
log g
log f

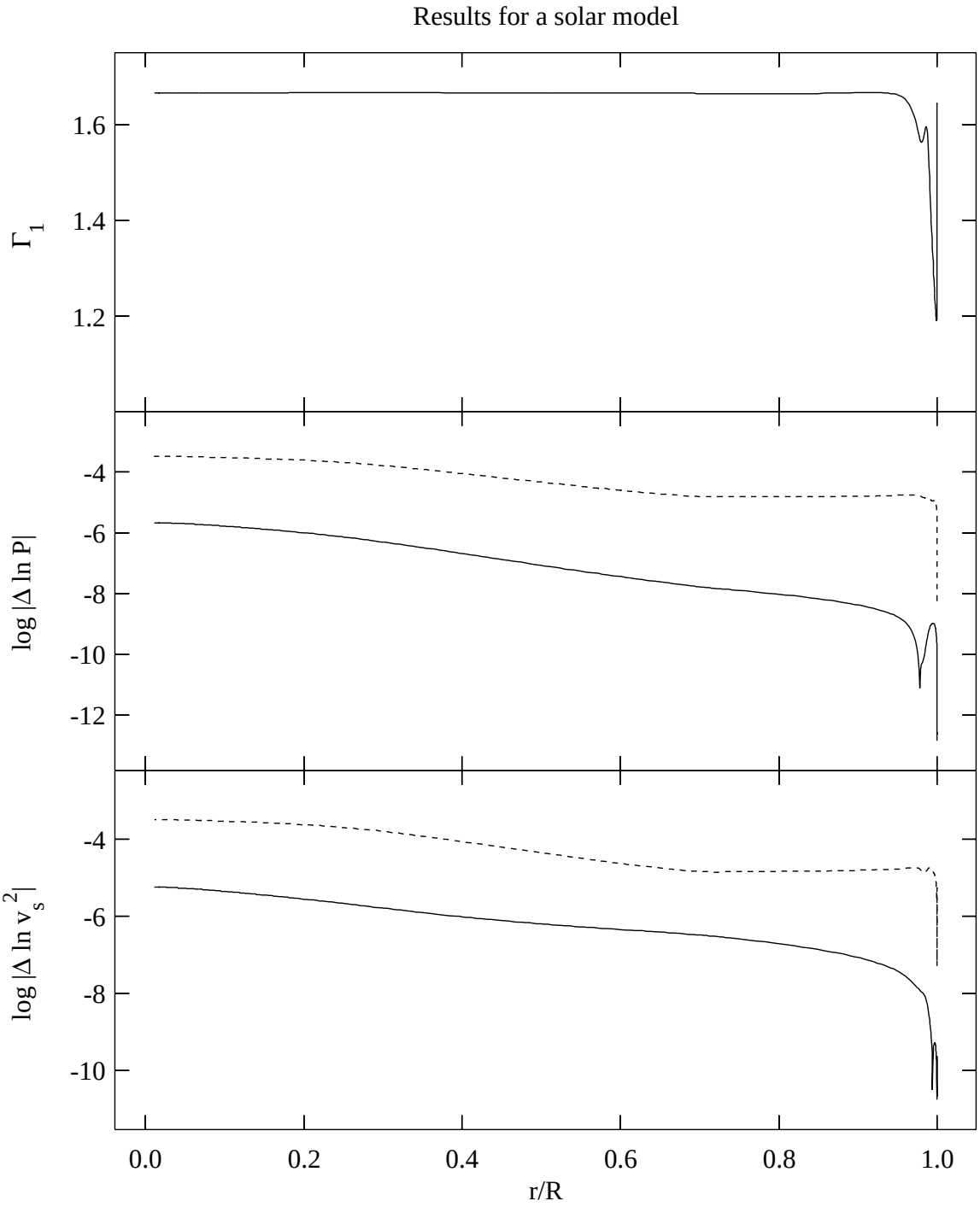
Results for a solar model
1.6
1.4
1.2
Γ_1
-4
-6
-8
-10
-12
log |Δ ln P|
-4
-6
-8
-10
log |Δ ln v_s^2|
0.0
0.2
0.4
0.6
0.8
1.0
r/R